

Evaluation of surfactant templates for one-pot hydrothermal synthesis of hierarchical SAPO-5

Daniel Ali^a, Caren Regine Zeiger^a, Muhammad Mohsin Azim^a, Hilde Lea Lein^b, Karina Mathisen^{a,*}

^a Department of Chemistry, Norwegian University of Science and Technology (NTNU), N-7491, Trondheim, Norway

^b Department of Materials Science and Engineering, Norwegian University of Science and Technology (NTNU), N-7491, Trondheim, Norway

ARTICLE INFO

Keywords:

Hierarchical
SAPO-5
Characterization
Zeotypes
Hydrothermal synthesis

ABSTRACT

Hierarchical SAPO-5 molecular sieves were synthesized with three different mesopore structure-directing agents (meso-SDAs) (cetyltrimethylammonium bromide (CTAB), myristyltrimethylammonium bromide (MTMAB) and [3-(trimethoxysilyl)propyl] dimethyloctadecylammonium chloride (TPOAC)) based on a soft-template hydrothermal synthesis procedure. To investigate the modified porosity of the hierarchical SAPO-5s, they were characterized thoroughly with the results being compared to the conventional microporous SAPO-5. Nitrogen sorption measurements revealed considerable hysteresis loops for the hierarchical SAPO-5s as well as larger mesopore volumes ($\geq 0.15 \text{ cm}^3 \text{ g}^{-1}$) compared to the conventional SAPO-5 ($0.05 \text{ cm}^3 \text{ g}^{-1}$). The relative number of acid sites for each sample was calculated from FTIR adsorption data and was in the order of C-SAPO-5 > H-CTAB > H-MTMAB > H-TPOAC. The hierarchical SAPO-5s had a significantly increased lifetime (>150 h) in the methanol to hydrocarbons (MTH) model reaction compared to the conventional SAPO-5 (<10 h), with TPOAC producing the most stable catalyst and MTMAB producing the catalyst with the largest product distribution. The modified porosity of the hierarchical SAPO-5s was additionally verified by an enhanced lifetime and increased production of large products in a shape selective process as well as a lower rate of coke formation compared to the conventional SAPO-5.

1. Introduction

The silicoaluminophosphate-5 (SAPO-5) with the AFI framework type is an acidic, microporous zeotype which is composed of 12-membered rings aligned in parallel, thus being a large-pore, one-dimensional structure where the micropores have a diameter of 7.3 \AA [1, 2]. Catalytically, SAPO-5 is a well-studied material known to be active in the isomerization of xylene, the methanol to hydrocarbons (MTH) reaction and in the cumene synthesis [3,4]. While the microporous SAPO-5 has unique shape selective properties, it suffers inherently from mass transfer limitations due to pore clogging (e.g. by coking) and generally low rates of diffusion [5,6]. In an effort to ameliorate this, the introduction of larger pores (typically mesopores) into the microporous structures to make so-called hierarchical materials has recently gained traction [7]. These hierarchical materials typically have a bimodal pore distribution where the larger mesopores are thought to act as diffusion highways for reactants and products to easily diffuse into and out of the

structure, respectively.

There are several pathways to make hierarchical SAPOs, often divided into either top-down or bottom-up approaches. Examples of the former include post-synthesis modification by e.g. dealumination or desilication, while examples of the latter include hard- or soft-templating techniques [8,9]. In the bottom-up approaches, the larger pore system is typically introduced into the structure during synthesis with large molecular templates or so-called structure-directing agents (SDAs). Several mesopore SDAs (meso-SDAs) have been employed as soft-templates during hydrothermal synthesis of hierarchical SAPOs, among which are the organosilane TPHAC ([3-(trimethoxysilyl)propyl] hexadecyldimethylammonium chloride) and the quaternary ammonium surfactant CTAB (cetyltrimethylammonium bromide) [3,10]. Danilina et al. [3] have previously attempted to do comparison studies between different surfactants (organosilane and quaternary ammonium), however syntheses with the quaternary ammonium surfactant did not yield phase pure SAPO-5 and the sample was therefore not further analyzed.

* Corresponding author.

E-mail address: karina.mathisen@ntnu.no (K. Mathisen).

<https://doi.org/10.1016/j.micromeso.2020.110364>

Received 3 April 2020; Received in revised form 19 May 2020; Accepted 26 May 2020

Available online 20 June 2020

1387-1811/© 2020 The Author(s). Published by Elsevier Inc. This is an open access article under the CC BY license (<http://creativecommons.org/licenses/by/4.0/>).

Consequently, there has yet to be a thorough characterization and comparison of the porosity resulting from applying different meso-SDAs for the synthesis of hierarchical SAPO-5.

In addition to alleviating diffusion limitations, the mesopores in hierarchical SAPOs may accommodate additional acid sites and increase the accessibility of acid sites located intrinsically in the micropores [11]. Consequently, these favourable properties may lead to increased catalyst lifetime, catalytic activity and product distribution [12]. Earlier studies on one-pot, hydrothermally synthesized hierarchical SAPO-5 using an organosilane surfactant as a meso-SDA for example, show that the hierarchical analogue displays a higher conversion and reaction rate for the alkylation of benzyl alcohol than its purely microporous counterpart [3]. Hierarchical SAPO-5 also shows an improved performance in the Beckmann rearrangement of bulky products [13] as well as a higher catalytic cracking activity for 1, 3, 5-triisopropylbenzene [11]. Studies done on other one-pot, hydrothermally synthesized hierarchical SAPOs such as SAPO-34 and SAPO-11, show similar trends. Hierarchical SAPO-34 synthesized with polymers as meso-SDAs for instance, displays an increased lifetime for the methanol to olefins (MTO) reaction while maintaining a conversion and shape selectivity that is comparable to that of the conventional microporous SAPO-34 [14,15]. As for SAPO-11, the bimodal pore system of hierarchical SAPO-11 synthesized with an organophosphate surfactant has been shown to significantly improve the mass transfer and selectivity towards more branched products for *n*-octane isomerization [16].

In this study, three different meso-SDAs (soft-templates) for the hydrothermal synthesis of hierarchical SAPO-5 were investigated and subsequently, the resulting porosity was evaluated and compared to the conventional SAPO-5. CTAB, MTMAB (myristyltrimethylammonium bromide) and TPOAC ([3-(trimethoxysilyl)propyl] dimethyloctadecylammonium chloride) were selected as meso-SDAs, where TPOAC was chosen as an organosilane surfactant for evaluation of template type, while CTAB and MTMAB were employed as quaternary ammonium surfactants for evaluation of the effects of template chain length.

The synthesized SAPO-5s were comprehensively analyzed to verify phase purity, surface and pore characteristics as well as properties of acid sites. The MTH reaction was employed as a model reaction to monitor the catalytic performance and product selectivity of the pore modified molecular sieves, while post-catalytic characterization was included to further characterize the pore topology.

2. Experimental

2.1. Synthesis of samples

2.1.1. Conventional SAPO-5

The conventional SAPO-5 was hydrothermally synthesized using a modification of the procedure described by Mathisen et al. [17]. An initial solution of pseudo-boehmite (Al_2O_3 , 5.00 g, Sasol, 71.8%) in deionized water (H_2O , 35.52 g) and orthophosphoric acid (H_3PO_4 , 8.12 g, Merck, 85%) was prepared and stirred for 3.5 h. Subsequently, colloidal silica AS-40 (SiO_2 , 2.13 g, Sigma Aldrich, 40 wt%) was added, and the resulting mixture was stirred for 45 min after which the microporous template, triethylamine (TEA, 4.25 g, Riedel-de Haën, purum), was introduced dropwise under stirring. The final gel, with a theoretical composition of 1.0Al: 1.0P: 0.2Si: 0.6TEA: 30 H_2O , was aged for 30 min under stirring before being poured into a 60 mL Teflon-lined stainless steel autoclave for crystallization at 200 °C for 24 h. After quenching, the resulting powder was washed four times with 150 mL deionized water. The final product was dried for 72 h at 70 °C in air, calcined at 550 °C for 5 h in air and labelled C-SAPO-5.

2.1.2. Hierarchical SAPO-5

Hierarchical SAPO-5 was synthesized by adding 0.05 equivalents of meso-SDA to the synthesis procedure of the conventional material (*vide supra*) where the meso-SDA was one of the following (see also Table 1):

cetyltrimethylammonium bromide (CTAB, Sigma Aldrich, >99%), myristyltrimethylammonium bromide (MTMAB, Sigma Aldrich, >99%) and [3-(trimethoxysilyl)propyl] dimethyloctadecylammonium chloride (TPOAC, Sigma Aldrich, 42 wt%). The meso-SDA was added dropwise after addition of the microporous template TEA. For CTAB and MTMAB, the template (e.g. CTAB, 1.25 g) was dissolved in heated deionized water (8.59 g, ~50 °C) prior to addition to the mixture. The water used for the template solution was subtracted from the initial amount of added water to maintain the composition ratio, which was 1.0Al: 1.0P: 0.2Si: 0.6TEA: 0.05meso-SDA: 30 H_2O for the final gels. The washing, drying and calcination procedures were the same as for the conventional SAPO-5, and labelling was done in the manner of "H" denoting hierarchical followed by the name of the meso-SDA used in the synthesis, resulting in the materials H-CTAB, H-MTMAB and H-TPOAC.

2.2. Characterization

X-ray powder diffraction (XRD) patterns were recorded on a Bruker D8 Focus X-ray Diffractometer with a $\text{CuK}\alpha$ radiation source (1.5406 Å) and LynxEye™ SuperSpeed Detector. The diffractograms were recorded from 5 to 60° with a step size of ~0.01°. A fixed 0.2 mm divergence slit was used throughout the run. Relative crystallinities were calculated according to the previously reported methods [18,19] using the following reflections of 2θ: 7.5°, 14.9°, 19.8°, 21.1°, 22.5° and 26.0°.

Nitrogen sorption analysis was performed on a Micromeritics Tristar 3000 Surface Area and Porosity Analyzer at -196 °C. The materials were degassed under vacuum at 250 °C prior to the measurements using a Micromeritics VacPrep 061 Sample Degas System in order to remove water and other volatile adsorbates. The specific surface area was determined by the BET (Brunauer-Emmett-Teller) method while the micropore and external area were estimated using the t-plot method. Finally, the specific pore volumes were obtained by BJH (Barrett-Joyner-Halenda) analysis.

Thermogravimetric analyses coupled with mass spectrometry (TGA-MS) were carried out with 10–15 mg of filtered particle size (212–425 μm) on a Netzsch Jupiter STA 449 equipped with a QMS 403 Aëlos quadrupole mass spectrometer. The flow consisted of 45 mL min⁻¹ air and 25 mL min⁻¹ argon while the temperature program started at 35 °C, subsequently heated to 550 °C at a rate of 2 °C min⁻¹ and held for 8 h before finally cooling down to room temperature at a rate of 2 °C min⁻¹.

Scanning electron microscopy (SEM) was performed on a Hitachi S-3400 N where the samples were gold coated by sputtering using an Edwards Sputter Coater (S150B) prior to imaging. Images were captured in secondary electron (SE) mode while particle sizes were determined using the software ImageJ (version 1.52a) [20].

Carbon monoxide (CO) adsorption was performed with a Bruker Vertex 80 FTIR spectrometer equipped with an LN-MCT detector from Kolmar Technologies and a custom-built transmission cell. Measurements were conducted at an aperture setting of 4 mm, a scanner velocity of 20 kHz and a resolution of 4 cm⁻¹. Samples were pressed into self-supported wafers (10–13 mg) and pre-treated for 1 h at 500 °C under vacuum to remove adsorbed water and impurities. Afterwards, the cell was cooled to -196 °C before slowly introducing CO (AGA). Finally, stepwise desorption of CO was conducted by gradually lowering the pressure in the system until the initial spectrum was recovered.

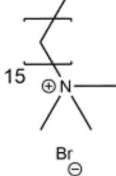
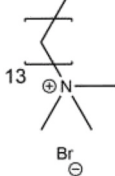
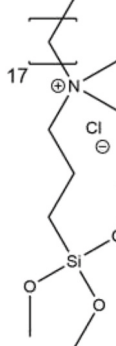
Inductively Coupled Plasma Mass Spectrometry (ICP-MS) was conducted using a High Resolution Inductively Coupled Plasma Element 2 in combination with an ICP-MS triple quad Agilent 8800. Samples (20–40 mg) were decomposed with concentrated nitric acid (HNO_3 , 1.5 mL, 65%) and concentrated hydrofluoric acid (HF, 0.5 mL, 40%). The final solutions were diluted with deionized water and filled into 16 mL sample tubes.

2.3. MTH model reaction

The methanol to hydrocarbons (MTH) model reaction was carried

Table 1

An overview of the surfactants employed as SDAs in this study and some of their known effects on the synthesis of SAPO materials.

Parameter	Surfactant property		
Abbreviation	CTAB	MTMAB	TPOAC
Name	Cetyltrimethylammonium bromide	Myristyltrimethylammonium bromide	[3-(trimethoxysilyl)propyl] dimethyloctadecyl ammonium chloride
Structure			
Surfactant type	Quaternary ammonium	Quaternary ammonium	Organosilane
Known effects on resulting materials	Controls particle size ^{a,b} [10,48, 56]	Controls particle size ^a [48]	Si-leaching [3,13]

^{a,b}Particle size effects are known [10,48,56] to occur for syntheses of SAPO-11^a and SAPO-34^b.

out in a tube reactor (ID: 4 mm). The reaction products were analyzed with a gas chromatograph equipped with a flame ionizing detector (FID) coupled to a mass spectrometer (GC-MS, Agilent 7890A coupled to an Agilent 5975C inert XL MSD).

In a typical experiment, 36 mg of filtered particle size (212–425 μm) of calcined SAPO-5 was loaded into the reactor before heating the reactor to 500 °C for 1 h to remove water and other adsorbed impurities. The reaction was performed at 400 °C by sending chilled methanol (0 °C, VWR, $\geq 99.8\%$) carried by helium into the reactor at a Weight Hourly Space Velocity (WHSV) of 1.8 $\text{g}_{\text{MeOH}}^{-1} \text{g}_{\text{cat}}^{-1} \text{h}^{-1}$.

3. Results

3.1. General characterization

Earlier reports on hydrothermally synthesized hierarchical SAPO-5 have shown that structural aspects such as phase purity [3] and sample matrix composition [13] may change or be influenced by the introduction of mesopores into the system. Danilina et al. [3] for example, found that the AFI phase collapsed when using a quaternary ammonium surfactant meso-SDA, while Newland et al. [13] found that using an organosilane surfactant produced a high silicon content hierarchical SAPO-5 due to silicon-leaching. As such, in order to evaluate how different meso-SDAs may affect the structural properties of hierarchical SAPO-5, a thorough general characterization is needed. Specifically, XRD was employed to confirm the phase purity and crystallinity of the samples, whereas ICP-MS was used to obtain information about the structural composition of the SAPOs. Nitrogen adsorption was used to provide invaluable information on the mesopore formation in the hierarchical SAPOs and finally, SEM was conducted to reveal the morphology of the samples as well as the particle size distributions.

The XRD patterns of the calcined conventional and hierarchical SAPO-5s are stacked together with the simulated AFI pattern in Fig. 1 [21].

The diffractograms of the SAPOs displayed a crystalline AFI phase and all hierarchical SAPOs were phase pure whereas the conventional SAPO showed a slight impurity (denoted with an asterisk in Fig. 1) ascribed to the competing CHA framework (SAPO-34) [22,23]. Furthermore, H-CTAB, H-MTMAB and H-TPOAC had slightly lower crystallinities (80, 77 and 85% respectively) when compared to

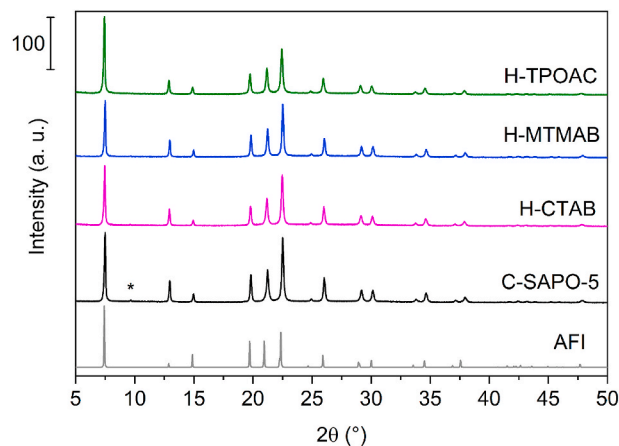


Fig. 1. XRD patterns of C-SAPO-5, H-CTAB, H-MTMAB and H-TPOAC with the AFI structure as a reference. The asterisk denotes a small impurity resulting from the competing CHA phase.

C-SAPO-5 (100%) as given in Table 2, which is in accordance to previous observations made for both hierarchical SAPO-5 and SAPO-34 [7,24, 25].

ICP-MS results (Table 2) revealed that the hierarchical SAPO-5 materials contained more than twice as much Si as the conventional SAPO did, with the amount of incorporated silicon decreasing in the order of H-TPOAC > H-CTAB \approx H-MTMAB > C-SAPO-5, where C-SAPO-5 had a Si/Al ratio of 0.07. While there are few reports on hydrothermal synthesis of hierarchical SAPO-5 with quaternary ammonium surfactants, a previous study on SAPO-34 showed that the Si/Al ratio of hierarchical SAPO-34 with CTAB as a meso-SDA was larger than the Si/Al ratio of the conventional SAPO [10]. The authors attributed this to an increased incorporation of Si on addition of CTAB. As CTAB and MTMAB both are quaternary ammonium surfactants and gave roughly the same Si/Al ratio in this study (~ 0.14), it is presumed that these surfactants facilitate the incorporation of Si in the SAPO-5 structure to a comparable extent. As for the organosilane surfactant, TPOAC gave a Si/Al ratio (0.31) that was larger than the theoretically calculated value (0.2). This has previously been reported for SAPO syntheses using TPOAC [26,27] and is most likely due to an interaction between the main silicon source (here

Table 2
Summary of XRD, ICP-MS and nitrogen sorption characterization results for the SAPO-5s.

Sample	RC ^a (%)	Si/Al _{theory} ^b Equivalents	Si/Al _{ICP} ^c	Surface area (m ² g ⁻¹)			Pore volume (cm ³ g ⁻¹)	
				S _{BET}	S _{micro}	S _{ext}	V _{micro}	V _{meso}
C-SAPO-5	100	0.2	0.07	280	222	58	0.11	0.05
H-CTAB	80	0.2	0.14	257	166	91	0.09	0.15
H-MTMAB	77	0.2	0.13	263	168	95	0.09	0.19
H-TPOAC	85	0.2	0.31	332	205	127	0.10	0.16

^a Relative crystallinity.

^b Theoretically calculated gel composition.

^c Sample composition obtained by ICP-MS element analysis for calcined samples.

colloidal silicon, AS-40) and the silicon head group of TPOAC.

The results from nitrogen adsorption analyses (Table 2) showed that the synthesized SAPO-5s had surface areas ranging from 257 to 332 m² g⁻¹, well within the reported range (245–377 m² g⁻¹) for this material in the literature [3,28,29]. Furthermore, the conventional SAPO-5 had a larger micropore area (222 m² g⁻¹) and a smaller external surface area (58 m² g⁻¹) than the hierarchical SAPO-5s. The total surface areas increased in the order of H-CTAB < H-MTMAB < C-SAPO-5 < H-TPOAC, where H-TPOAC had the largest total (332 m² g⁻¹) and external surface area (127 m² g⁻¹). H-TPOAC also deviated from the other hierarchical SAPO-5s by being the only hierarchical sample that had a larger total surface area than the conventional SAPO-5 (280 m² g⁻¹), matching previous reports on hierarchical SAPO-5 synthesized with organosilane surfactants [3,27]. On the other hand, the lower total surface areas of H-CTAB (257 m² g⁻¹) and H-MTMAB (263 m² g⁻¹) were comparable to a previous study on hierarchical SAPO-34 with a quaternary ammonium surfactant (CTAB) as a meso-SDA [30], where increasing the content of CTAB corresponded to a decrease in the total surface area.

As for the pore volumes, the micropore volumes of the SAPO-5s were quite similar (ranging from 0.09 to 0.11 cm³ g⁻¹), however the hierarchical SAPO-5s displayed more than three times the mesoporous volume (0.15–0.19 cm³ g⁻¹) compared to the conventional SAPO-5 (0.05 cm³ g⁻¹) which has also been observed in the literature [3,27]. Notably, even though H-TPOAC had the largest external surface area of 127 m² g⁻¹, H-MTMAB had the greatest mesopore volume of 0.19 cm³ g⁻¹. It should be noted that even though the surface areas of H-TPOAC matched literature reports, the mesopore volume (0.16 cm³ g⁻¹) was in the lower range of what has previously been reported (0.16–0.30 cm³ g⁻¹) for hierarchical SAPO-5 synthesized with TPOAC [13,27]. Collectively, the increased external surface areas and mesopore volumes of the hierarchical SAPO-5s compared to the conventional SAPO-5 strongly suggest the presence and incorporation of mesopores into the hierarchical structures [3].

The BET isotherms of the SAPO-5 samples are given in Fig. 2A, while Fig. 2B gives an overview of the pore size distributions. Generally, the isotherms were altogether comparable to the ones shown in literature [3,31]. C-SAPO-5 displayed a type Ia isotherm, characteristic for materials with narrow micropores, with a small H4 hysteresis loop, characteristic for aggregated SAPO particles or the presence of mesoporosity, as defined by IUPAC [32]. The isotherms for H-CTAB and H-MTMAB were quite similar and matched a plateau-less type IV isotherm, characteristic for meso- and macroporous adsorbents. The hysteresis loops for both samples were composites of H3 and H4 loops, where H-CTAB showed a larger influence of the H4 hysteresis loop, while H-MTMAB showed a larger influence of the H3 hysteresis loop which typically indicates the presence of macroporosity [32]. The isotherm of H-TPOAC was a composite of type I and II with an H4 hysteresis loop, again indicating the presence of voids among aggregated particles or mesoporosity.

Regarding the pore size distributions (Fig. 2B), C-SAPO-5 showed a typical pore size distribution for microporous materials with no prominent features and pores wider than 2 nm were ascribed to intercrystalline voids between the particles. For the hierarchical samples, H-

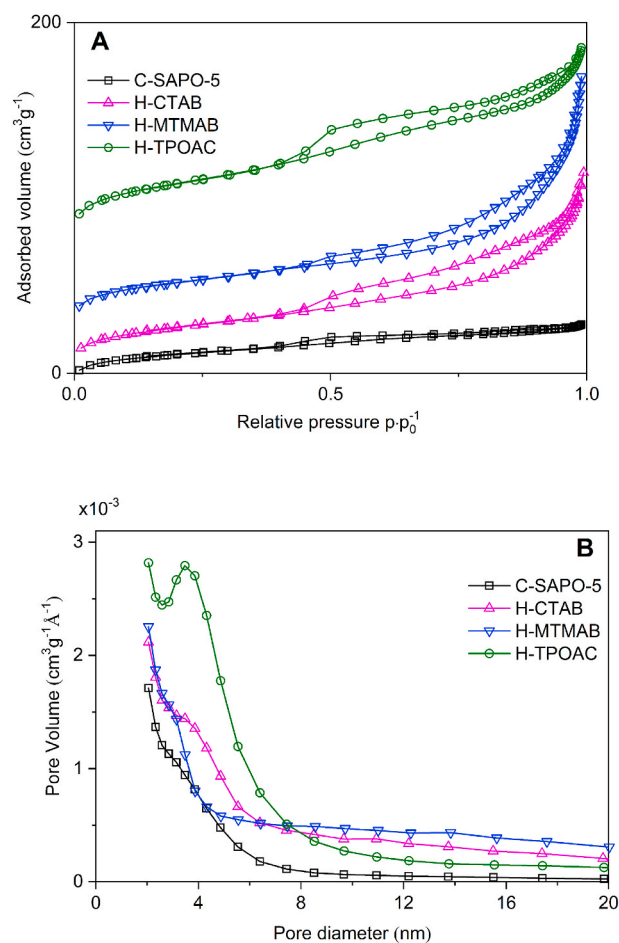


Fig. 2. Nitrogen sorption isotherms (A) and pore size distributions (B) for all synthesized SAPO-5s. For the pore size distributions, the adsorption branch of the BJH method was used.

TPOAC displayed a clear maximum at a pore width of 3.5 nm, while H-CTAB and H-MTMAB both displayed a shoulder at 3.5 and 3.0 nm, respectively, possibly indicating the presence of aptly sized mesopores. Others have reported similar results when using CTAB and TPOAC as SDAs for synthesizing hierarchical SAPO-5 [13,33].

The SEM images of the synthesized SAPO-5s are shown in Fig. 3. The average particle sizes matched previous reports [3] and were 21, 19, 23 and 18 μm for C-SAPO-5, H-CTAB, H-MTMAB and H-TPOAC, respectively. All samples displayed agglomerates of smaller plate-like or hexagonal rod-like particles which is in good accordance with the literature reports [2,31].

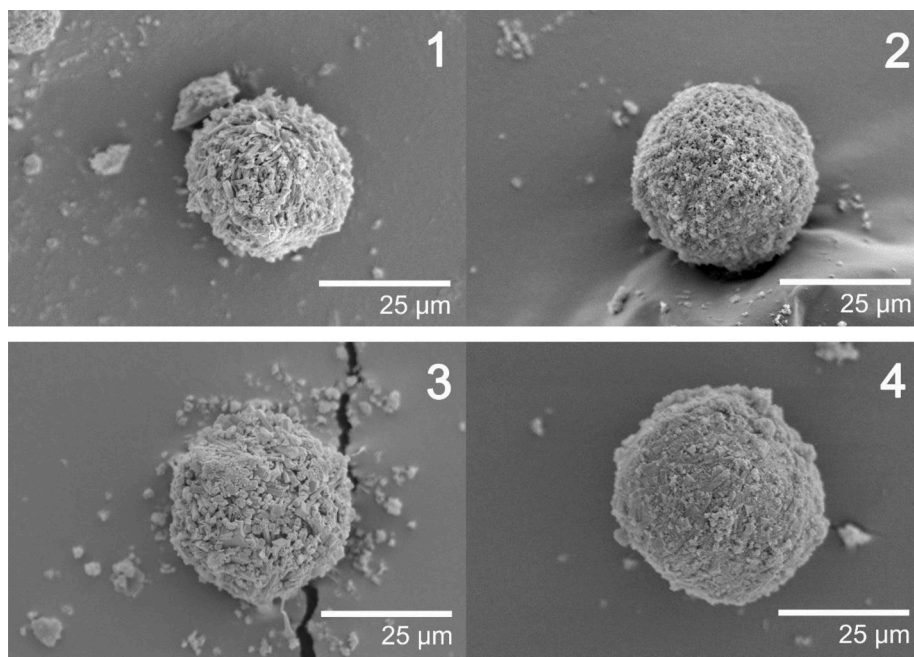


Fig. 3. SEM micrographs of C-SAPO-5 (1), H-CTAB (2), H-MTMAB (3) and H-TPOAC (4), showing a typical particle for each sample.

3.2. Acid characterization by FTIR spectroscopy with CO adsorption

Previous reports on the SAPO-5 system [13,24] have indicated that the number of acid sites may decrease when modifying porosity for the purpose of creating hierarchical systems. Thus, in order to determine if the introduction of mesopores to SAPO-5 altered the number and strength of acid sites, the acid properties of the SAPOs were characterized using CO as a molecular probe.

The results of the CO adsorption are depicted in Fig. S1 as normalized difference spectra, where the clean vacuum spectra before CO adsorption have been subtracted from the spectra fully perturbed by CO. All samples displayed the typically reported bands [29,34] for SAPO-5: silanol (Si-OH) sites at 3745 cm^{-1} , surface groups (terminal P-OH/Al-OH) at 3679 cm^{-1} , high frequency Brønsted acid sites (BAS) at approximately 3629 cm^{-1} and low frequency BAS at 3515 cm^{-1} . It should be mentioned that H-MTMAB had BAS located at a slightly higher frequency ($\sim 3641\text{ cm}^{-1}$) compared to the other samples. The high frequency BAS are situated in the larger 12-membered rings while the low frequency BAS are situated in the smaller 6-membered rings of SAPO-5 which were found to be inaccessible to CO, in accordance with previous reports [4,29,34].

Table S1 gives an overview of the location of the observed bands for each sample and the shifts, $\Delta\nu_{OH}$, between the high frequency BAS ($\nu_{Brønsted}$) and the BAS perturbed by CO ($\nu_{Brønsted}^*$). The shifts of the samples were found to be between 254 cm^{-1} and 266 cm^{-1} , where a BAS shift between 254 and 268 cm^{-1} is an average value for SAPO-5 according to the literature reports [4,35]. Thus, the acid strength of SAPO-5 was not significantly affected by the introduction of mesopores, matching previous reports [3] on the hierarchical SAPO-5.

By integrating the area under the peaks of the FTIR spectra and setting the number of sites present in the conventional sample to 1, a relative estimate on the total number of acid sites in each sample was obtained (Table S2). The conventional SAPO-5 contained the most BAS, matching earlier reports [13], followed by H-CTAB, H-MTMAB and H-TPOAC (0.55, 0.22 and 0.15, respectively). Whereas all samples contained approximately the same number of surface groups, H-TPOAC contained a slightly higher relative number of silanol groups (1.01) compared to H-CTAB and H-MTMAB (0.77 and 0.81, respectively). Conclusively, while the silanol groups are affected to a varying degree,

the introduction of mesopores causes a considerable drop in the total number of Brønsted acid sites that is larger than previous reports on hierarchical SAPO-5 [24].

3.3. Methanol to hydrocarbons (MTH) model reaction over SAPO-5

The activity of a catalyst in the MTH reaction depends on many factors including acid strength, acid density, acid site location, particle size and pore topology [28,36–39]. While the acid strength and density as well as the particle size may be evaluated using other techniques (*vide supra*), the pore topology and acid site location may be evaluated by utilizing the MTH reaction. Specifically for this model reaction, the modification of the pore topology by introduction of intraconnected mesopores and micropores may result in alleviated diffusion limitations and reduced deactivation as coke precursors may easily diffuse out of the system, leading to an increased catalyst lifetime [7]. Furthermore, should the Brønsted acid sites be situated in, or close to, spacious mesopores, the product distribution of the MTH reaction may be shifted towards the formation of larger products [38,39]. Finally, the presence of weak acid sites (silanols) in spacious mesopores may also increase the lifetime of reactions that utilize these weak acid sites [13], e.g. the dehydration of methanol to dimethylether (DME) [28,40]. Thus, the methanol to hydrocarbons reaction was used to elucidate the pore topology of the hierarchical samples as well as to get a preliminary indication of the acid site locations in the samples.

The methanol conversion for the samples is displayed in Fig. 4. The catalysts were deemed to be deactivated after falling below an arbitrarily chosen conversion of 60%.

The stability and lifetimes of the hierarchical SAPO-5 samples were greatly enhanced compared to the conventional SAPO-5 sample. Specifically for the samples C-SAPO-5, H-CTAB, H-MTMAB and H-TPOAC, the corresponding initial conversions were 82%, 82%, 86% and 78%, while the 20 h conversions were 47%, 77%, 76% and 80%, respectively. Even though the initial conversion and lifetime of the conventional SAPO-5 matched previous reports at similar conditions [4], the hierarchical SAPOs had more than ten times the conversion of the conventional SAPO after ~ 110 h on stream. The minor differences in stability within the hierarchical SAPO-5 samples indicated that H-TPOAC was the most stable catalyst followed by H-CTAB and finally H-MTMAB.

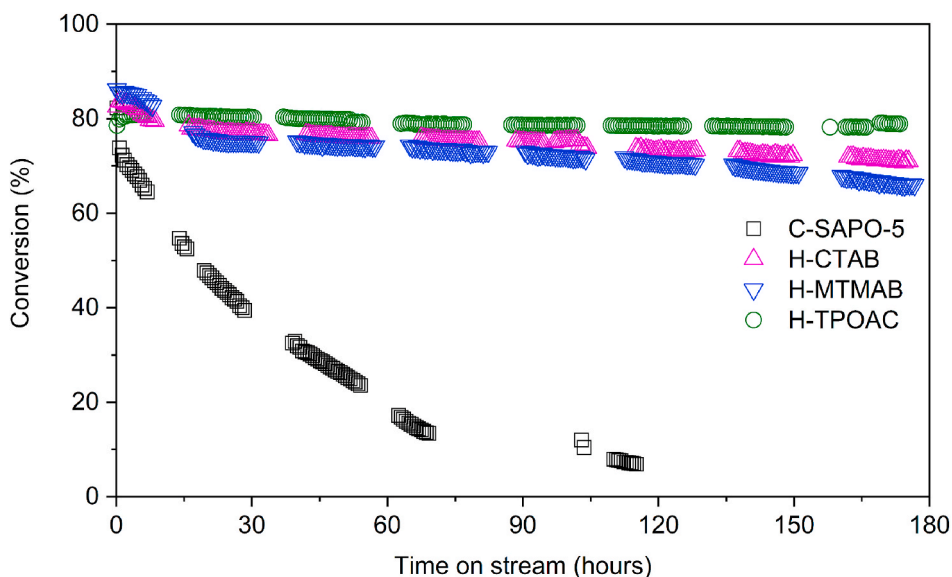


Fig. 4. Methanol conversion for C-SAPO-5, H-TPOAC, H-CTAB and H-MTMAB.

Nevertheless, the hierarchical samples predominantly retained their stability and high activity even after 180 h on stream, whereas C-SAPO-5 deactivated after approximately 10 h on stream.

As for the product distribution, the hierarchical samples all produced larger and more branched products than C-SAPO-5, ranging from branched polymethylbenzenes (e.g. 1-ethyl-2,3,4,5,6-pentamethylbenzene) to heavily methylated naphthalenes (e.g. 4-(1-methylethyl)-1,6-dimethylnaphthalene). Furthermore, H-CTAB and H-MTMAB produced significantly increased amounts of polymethylbenzenes (peak values of 17% and 35%, respectively) as further evidenced by Fig. 5 and Table S3. The minimal production of polymethylbenzenes for the conventional SAPO-5 (peak value of 11%, see Fig. S2) matched previous reports conducted at various conditions [4,41,42], further solidifying the exceptional properties of the hierarchical SAPO-5s.

3.4. Post-catalysis characterization

To further elucidate the pore topology of hierarchical SAPO-5, several post-catalysis characterizations were performed. Post-catalysis XRD was done in order to exclude phase collapse as a reason for deactivation, while nitrogen sorption would clarify if the pores of the SAPO-5 were congested. Finally, TGA-MS was performed to quantify the amount of retained coke in the samples after the MTH model reaction as well as to calculate the rate of coke formation.

Post-catalysis XRD showed that albeit losing some crystallinity, the major phase for all samples was still the AFI phase (Fig. S3), confirming that the samples did not collapse during the reaction. Nitrogen adsorption on spent samples (Fig. 6) confirmed that the conventional SAPO-5's pores were indeed completely congested, whereas the hierarchical samples H-TPOAC and H-CTAB retained at least 50% of their initial external surface areas and 60% of their initial mesoporous volumes. For H-MTMAB however, the retained external surface area and mesoporous volume was less than 30%, indicating that a significant portion of the mesopores in the catalyst had been congested.

The initial mass loss observed in the TGA-MS results after catalysis (Fig. S4) was attributed to the loss of water, while the second and larger mass loss occurring after approximately 250 min (~ 500 °C) was attributed to the oxidation and loss of coke as carbon dioxide (CO_2 , $m/z = 44$). With these considerations, the conventional SAPO-5 lost more water and less coke (approximately 8.6%) than the hierarchical SAPO-5s (approximately 10%). Furthermore, when considering the total reaction time for the catalysts it becomes clear that the generation of coke per

hour (Table S4) was much lower for the hierarchical samples ($0.01\text{--}0.02 \text{ mg}_{\text{coke}} \text{ h}^{-1}$) compared to the conventional sample ($0.03 \text{ mg}_{\text{coke}} \text{ h}^{-1}$).

4. Discussion

The main goal of this study was to characterize and compare the porosities of hierarchical SAPO-5 synthesized with different meso-SDAs to each other, and to the conventional SAPO-5. The discussion will be divided in three parts where firstly, the structural effect of the inclusion of the three meso-SDAs will be discussed as well as whether or not these meso-SDAs in fact produced hierarchical SAPO-5 samples. Secondly, the pore topology of the SAPO-5 catalysts will be discussed in conjunction with the activity and location of the weak acid sites (WAS, silanols). Finally, the product distribution from the methanol to hydrocarbons (MTH) reaction will be considered together with the Brønsted acid site (BAS) location in the SAPO-5 samples.

4.1. Evaluation of various meso-SDAs for synthesis of hierarchical SAPO-5

In this study, three different meso-SDAs, CTAB, MTMAB and TPOAC, were employed for the synthesis of hierarchical SAPO-5. The meso-SDAs were chosen and compared in such a way that the effect of template chain length and template type could be studied. The former was evaluated by comparing the slightly longer chained surfactant CTAB to the shorter MTMAB, while the latter was evaluated by comparing the quaternary ammonium surfactants CTAB and MTMAB to the organosilane surfactant TPOAC.

The relative crystallinities, Table 2, did not differ significantly between the three meso-SDAs and all hierarchical SAPO-5s were of comparably high purity and crystallinity ($\sim 80\%$). As for the textural properties, the quaternary ammonium surfactants (CTAB and MTMAB) produced SAPO-5 with similarly small overall surface areas ($\sim 260 \text{ m}^2 \text{ g}^{-1}$) compared to the organosilane surfactant TPOAC ($332 \text{ m}^2 \text{ g}^{-1}$), suggesting that organosilane surfactants are favourable for synthesizing large surface area hierarchical SAPO-5. Interestingly, while H-TPOAC also displayed the largest external surface area, H-MTMAB had the largest mesopore volume. While the mesopore volume of H-TPOAC (*vide supra*) was in the lower region of earlier reports on hierarchical SAPO-5 [13,27], the increased mesopore volume of H-MTMAB may also be due to the wider distribution of mesopores for H-MTMAB as seen from the BJH in Fig. 2. In fact, both H-CTAB and H-MTMAB had a wider

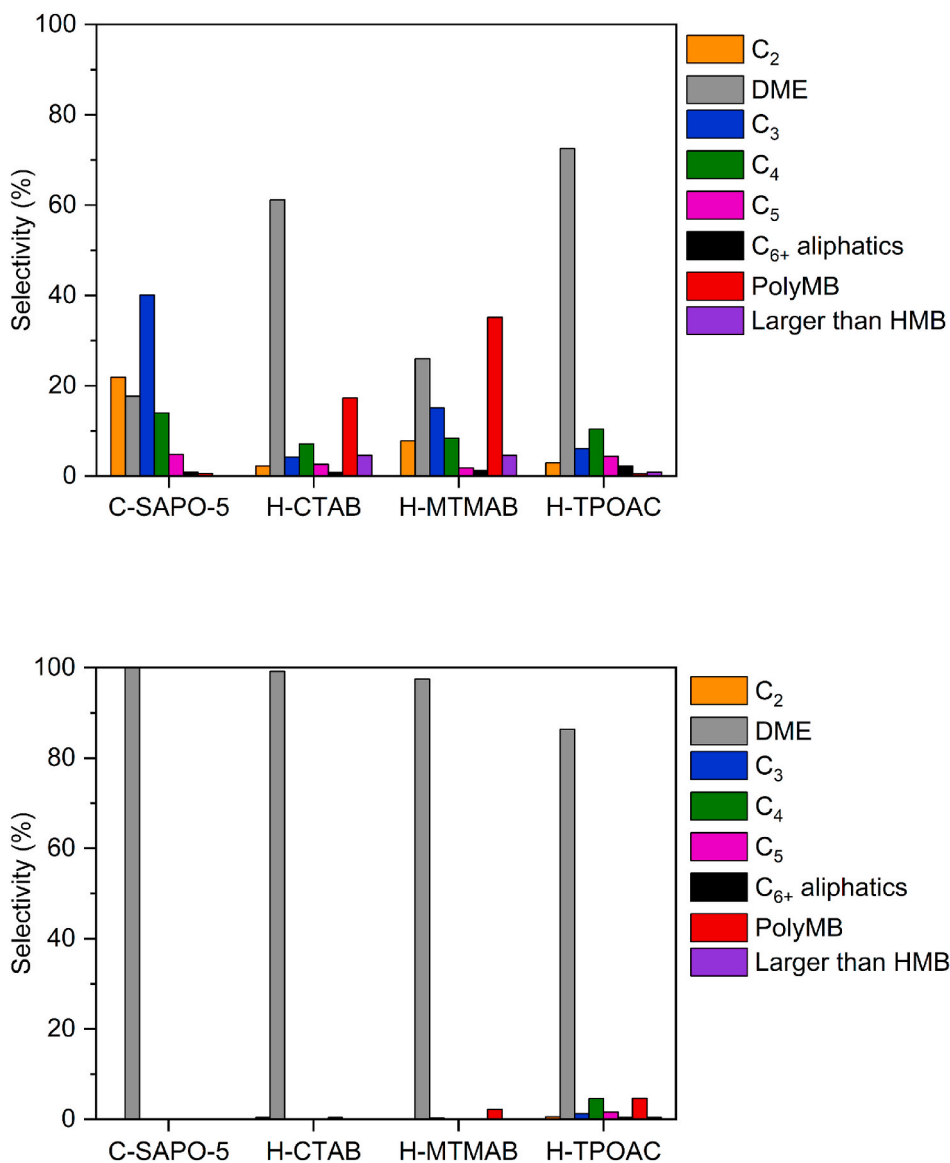


Fig. 5. Initial (top) and 20 h (bottom) product distributions for the MTH model reaction, where ‘PolyMB’ are polymethylbenzenes (tetra-, penta- and hexamethylbenzene (HMB)). Detailed values have been given in Table S3 in the supplementary information.

distribution of mesopores compared to H-TPOAC, which had a relatively uniform distribution of mesopores.

The total number of Brønsted acid sites in the SAPO-5 system is related to the average acid strength of the system, with earlier studies [33,43–46] reporting an increase in acid strength as the number of Brønsted acid sites is increased. On the other hand, one study [47] reported a decrease in acid strength as the number of Brønsted acid sites increased, while another study [13] reported no change in the acid strength as the number of Brønsted acid sites changed. The total number of Brønsted acid sites in SAPO-5 is also related to the amount of incorporated silicon in the system, with previous reports [46,47] indicating that an increased incorporation of Si causes a reduction in the total number of acid sites. The incorporation of large amounts of silicon may also form silica islands, decreasing the number of acid sites while the acid strength remains the same [28,46].

For the hierarchical SAPO-5s made with quaternary ammonium surfactants, CO adsorption showed that H-MTMAB had fewer acid sites (0.22) than H-CTAB (0.55) and a slightly increased acid shift (Table 3). This is contradictory to what previous comparisons [48] between CTAB and MTMAB as SDAs for SAPO-11 have shown, where MTMAB produced

the SAPO-11 with the largest number of Brønsted acid sites. Regarding the increased acid shift of H-MTMAB, the results match one previous report [47] claiming that when the number of acid sites in the SAPO-5 system decreases, the average strength of the acid sites increases. This apparent trend in acid strength is not applicable for H-TPOAC however, which through CO adsorption was shown to have fewer acid sites (0.15) than H-MTMAB but a similar acid shift, thus matching a previous report [13] indicating that the acid strength remains constant regardless of the number of acid sites in the samples.

Moreover, ICP-MS results showed that the hierarchical SAPO-5s had more incorporated silicon than the conventional SAPO-5. An increased incorporation of silicon has as mentioned been shown to cause a reduction in the number of Brønsted acid sites [46,47]. Thus, rather than directly being an effect of the introduction of mesopores, it is likely that the increased incorporation of silicon in the hierarchical SAPO-5s has contributed to the loss of Brønsted acid sites for these samples. Furthermore, CO adsorption indicated that H-TPOAC had slightly more silanol groups than H-CTAB and H-MTMAB. This indicates the presence of silica islands or perhaps an increased amount of silanol sites situated within the mesopores [13]. It is therefore possible that the reduced

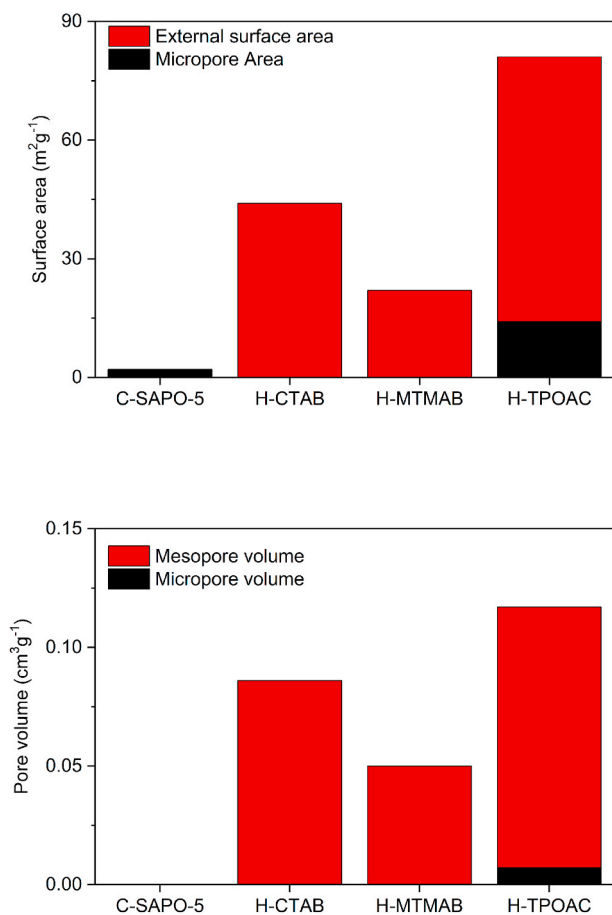


Fig. 6. Results from surface area (top) and pore volume (bottom) measurements via nitrogen adsorption on spent SAPO-5 samples.

number of Brønsted acid sites for H-TPOAC is also due to the presence of a larger number of silanol sites compared to H-CTAB and H-MTMAB.

In summary, the employed surfactants produced crystalline SAPO-5 with a significant portion of mesopores, as indicated by the textural properties. The number of Brønsted and weak acid sites differed according to surfactant type and chain length, where the long chained quaternary ammonium surfactant CTAB gave the largest number of BAS, followed by MTMAB and finally the organosilane surfactant TPOAC, giving the smallest number of BAS but the largest number of weak acid sites.

4.2. Activity and location of WAS and pore topology of hierarchical SAPO-5

The lifetime of a catalyst in the MTH reaction mainly depends on the factors given in Table 4, namely the acid strength, acid density, particle size and pore topology [28,36–38]. While a higher acid strength and density is known to cause a rapid catalyst deactivation due to an increased production of coke, smaller particles increase the lifetime of the catalyst [28,37,38]. Moreover, whereas the production of

hydrocarbons in the MTH reaction is mainly catalyzed by BAS, the production of DME proceeds at weaker acid sites (WAS) such as silanols and surface groups [28,40]. As these weaker acid sites only catalyze the simple dehydration of methanol, they are not expected to be directly blocked by deposits of carbonaceous species, i.e. coke. In the micropores of a conventional SAPO however, WAS may be indirectly blocked by coke produced by the stronger BAS, leading to pore congestion and a shorter lifetime for DME production. On the other hand, if WAS are also located in spacious mesopores, the lifetime of DME production would be expected to increase due to limited pore congestion.

When comparing the lifetimes of the catalysts for DME production, it becomes clear that all hierarchical SAPO-5 samples have a much longer lifetime than the conventional SAPO-5, with H-TPOAC being the most stable catalyst. Hajfarajollah et al. [42] reported that for SAPO-5 catalysts in the methanol to olefins (MTO) reaction, an increased lifetime may be expected for smaller particles, however SEM results showed that the average particle size of the samples in this study were of similar size (~20 μm). The variations in acid strength are likely not a factor here either as the acid shifts of the samples in this study are quite similar, in particular when considering that the isotopological SSZ-24 zeolite has an acid shift of 317 cm⁻¹ [49]. The relative number of acid sites however, indicates that the conventional SAPO-5 has a larger number of BAS than the hierarchical SAPO-5s. As previously mentioned, an increased density of acid sites is known to cause a more rapid catalyst deactivation due to a larger production of coke [38], however this alone does not explain why the production of DME decreased rapidly for C-SAPO-5. Post-catalysis nitrogen adsorption results (Fig. 6) indicated that the micropores in fact were congested and as expected, the observed deactivation of C-SAPO-5 was caused by weak acid sites in the micropores being blocked due to production of coke by the stronger BAS. On the other hand, for the hierarchical SAPO-5s the conversion and production of DME was more or less stable for over 150 h. Post-catalysis nitrogen adsorption (Fig. 6) indicated that the hierarchical samples retained a relatively large portion of their external surface areas and mesoporous volumes after the catalytic reaction. These results may be explained by recognizing the presence of easily accessible weak acid sites in the spacious mesopores of H-CTAB, H-MTMAB and H-TPOAC.

As a final note on pore topology, previous reports on the rate of coke formation in the MTH reaction [14,15], show that hierarchical SAPOs with an intracrystalline pore structure have decreased rates of coke formation compared to their microporous analogues. This is typically attributed to the reduction of mass transfer limitations by the presence of larger, intracrystalline mesopores in the hierarchical systems which allow coke precursors to promptly diffuse out of the micropores. In other words, a low rate of coke formation suggests intraconnectivity between the micro- and mesopores, where the latter should also be accessible from the surface of the catalyst particle. Thus, the formation rate of coke would be expected to be lower for hierarchical systems than for purely microporous systems due to an increased mass transport throughout the hierarchical systems [50].

Specifically for SAPO-5, deactivation in the MTH reaction has been shown to occur due to accumulation of coke through blockage of the one-dimensional pore network by formation of large molecules [51]. The presence of intracrystalline mesopores would allow these large molecules to diffuse out of the structure, thus reducing the formation rate of coke. Promisingly, the hierarchical SAPO-5s had lower rates of

Table 3
Summary of SEM and FTIR characterization results for the SAPO-5s.

Sample	Particle size (μm)	BAS shift ($\Delta\nu_{OH}$, cm ⁻¹)	ρ^a (BAS) (a.u.)	ρ (WAS) (a.u.)
C-SAPO-5	21	254	1	1
H-CTAB	19	258	0.55	0.77
H-MTMAB	23	266	0.22	0.81
H-TPOAC	18	264	0.15	1.01

^a Relative density of acid sites.

Table 4

An overview of the parameters known to affect a catalyst's activity, lifetime and large product selectivity in the MTH reaction as well as how they relate to the SAPO-5s synthesized in this study.

Parameter	Activity	Lifetime	Large product selectivity ^a	For SAPO-5s in this study
(Increased) density of BAS [28, 38, 39]	↑	↓	↑	SDA dependent
BAS in spacious pores (acid site location & pore topology) [38, 39, 49]	-	-	↑	For verification
WAS in spacious pores (DME production) ^b [13]	-	↑	-	For verification
(Increased) acid strength [28, 38, 49]	↑	↓	↑	Constant
(Smaller) particle size ^c [28, 37, 42, 52]	-	↑	↑	Constant
Hierarchical pore topology [7, 14, 15]	-	↑	-	For verification

^aProducts larger than C₅ and aromatic hydrocarbons

^bBased on results from the Beckmann rearrangement by Newland et al. [13].

^cSpecifically for SAPO-5, no significant differences in C₅ and aromatic product selectivity have been observed for different particle sizes [28, 42].

coke formation (Table S4) compared to the conventional SAPO-5, further solidifying the presence of alleviated diffusion limitations and pore intraconnectivity.

4.3. Product distribution of the MTH reaction and BAS location in hierarchical SAPO-5

The main factors that affect the product distribution in the MTH reaction are the particle size, pore topology, acid site location, acid strength and acid density (see also Table 4) [39,42,49,52]. Specifically for the SAPO-5 however, Hajfarajollah et al. [42] did not observe any significant variation in the product distribution of DME nor aromatics for differently sized SAPO-5 particles. As for the pore topology, the size of the pore channels and apertures influences the size of the products that are able to enter, pass through and exit the structure [49]. For the conventional SAPO-5, the product distribution typically ranges from ethene as the smallest product, to hexamethylbenzene (HMB, kinetic diameter of ~8 Å [53,54]) as the largest and most branched product that is observed in significant quantities [4,55]. For structures with more space due to cages and/or cavities, e.g. mordenite (MOR), larger products such as 2-ringed aromatics (naphthalenes) may form in small quantities [39]. Similarly, products larger than HMB may form in the hierarchical SAPO-5 provided that Brønsted acid sites are present in the mesopores. Furthermore, the product distribution is also highly dependent on the acid strength of the catalyst [4,28]. The production of aromatics for instance, is typically associated with elevated acid strength, and the strongly acidic AFI zeolite SSZ-24 has previously been reported [49] to produce larger amounts of aromatics than the conventional SAPO-5. As previously mentioned however, the acid shifts of the samples in this study are quite similar, especially when compared to more acidic isostructural zeolites [49]. The same authors also concluded that for SAPO-5, the product selectivity in the MTH reaction is not

significantly influenced by differences in acid density [49].

To summarize and as Table 4 outlines, considering that the acid strengths and particle sizes of the SAPO-5s synthesized in this study are constant, any differences in the product distribution cannot be ascribed to variations in these parameters. Finally, as differences in acid density do not affect the product distribution of the SAPO-5 system [49], a potential discrepancy in the product distribution between the conventional and hierarchical SAPO-5s has to be caused by the location of the BAS.

While the initial products for the conventional SAPO-5 were principally light olefins (propene and ethene), all hierarchical samples produced significant quantities of DME and the quaternary ammonium surfactant-synthesized H-CTAB and H-MTMAB produced considerable quantities of polymethylbenzenes as well. More importantly and as previously mentioned, the hierarchical SAPO-5s produced larger products than what was expected of the AFI framework, including branched polymethylbenzenes (e.g. 1-ethyl-2,3,4,5,6-pentamethylbenzene) as well as heavily methylated naphthalenes (e.g. 4-(1-methylethyl)-1,6-dimethylnaphthalene). This indicates that a portion of the Brønsted acid sites must be located inside the mesopores, especially for H-CTAB and H-MTMAB, with peak production values reaching 8% and 14% respectively compared to 1.5% for H-TPOAC (Fig. 7).

The product distribution in Fig. 7 shows that both H-CTAB and H-MTMAB produce significantly larger quantities of larger products compared to H-TPOAC. Furthermore, while H-TPOAC produces less overall hydrocarbons, the catalyst has a larger initial production of DME compared to H-CTAB and H-MTMAB (Fig. 5). This may suggest that the organosilane surfactant TPOAC promotes the formation of silanols in the mesopores rather than BAS, which seems to be more prevalent for the quaternary surfactants. The post-catalysis nitrogen adsorption results (Fig. 6) further substantiate this assumption, indicating that the mesopores of H-MTMAB and H-CTAB are more congested than that of H-TPOAC. This is most likely the result of H-MTMAB and H-CTAB having a

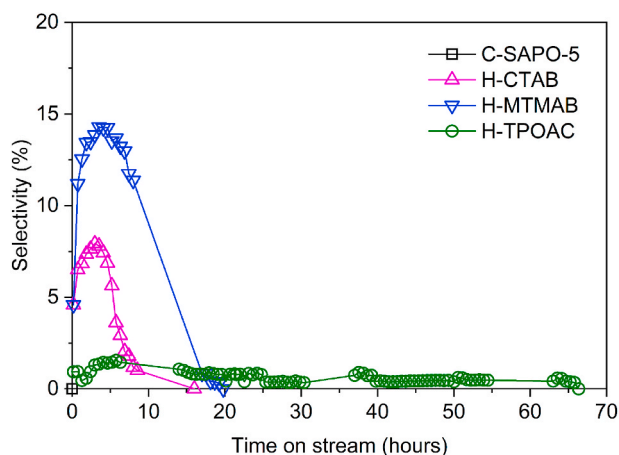


Fig. 7. Selectivity of products larger than hexamethylbenzene in the MTH reaction for C-SAPO-5, H-CTAB, H-MTMAB and H-TPOAC.

larger number of BAS located in the mesopores compared to H-TPOAC.

Interestingly, although the quaternary surfactants used for synthesis were fairly similar, there was a substantial difference in the product distribution for H-CTAB and H-MTMAB. Clearly, both H-CTAB and H-MTMAB produced considerable quantities of products larger than HMB compared to the other catalysts, however H-MTMAB produced almost twice as much as H-CTAB. Even though Guo et al. [48] did comparison studies on SAPO-11 synthesized with CTAB and MTMAB, they did not observe such a dramatic difference in the product distribution of *n*-octane isomerization over SAPO-11. This is a significant result, as the main difference between H-CTAB and H-MTMAB in this study was the variation in surfactant length between CTAB and MTMAB, suggesting that this variation caused a fundamental shift in the properties of the synthesized hierarchical SAPO-5s. This, as previously mentioned, is further reflected in the post-catalysis nitrogen adsorption (Fig. 6) and TGA-MS measurements (Fig. S4), where H-MTMAB both had a lower retained overall surface area as well as a lower generation of coke compared to H-CTAB. Conclusively, it is likely that the short-chained surfactant MTMAB produces a hierarchical SAPO-5 with both a better intra-connectivity of the pore network, and a greater number of BAS situated in the mesopores compared to CTAB and TPOAC.

5. Conclusion

The XRD results confirmed that the AFI structure was obtained in all the SAPO-5 samples and the BET results confirmed the presence of both micropores and mesopores for the hierarchical SAPO-5s. While CO adsorption confirmed that comparably strong acid sites were present in all samples, the relative number of acid sites in the samples varied according to the type and length of meso-SDA that was used, with the quaternary ammonium surfactant CTAB giving the largest and organosilane surfactant TPOAC giving the smallest number of Brønsted acid sites. The catalytic results demonstrated the exceptional properties of the mesopores in the hierarchical SAPOs through a considerably increased lifetime and production of larger products than the conventional SAPO-5. Post-catalysis TGA-MS furthermore indicated that the hierarchical SAPO-5 samples had lower rates of coke formation compared to the conventional analogue. In combination with the catalytic findings, this suggested that the mass transfer limitations were reduced due to an overall better diffusion throughout the hierarchical catalyst particles, correspondingly indicating the presence of intra-connected micro- and mesopores in the hierarchical SAPO-5s. Lastly, the quaternary ammonium surfactants seemed to direct the formation of Brønsted acid sites towards the mesopores to a greater extent compared to the organosilane surfactant TPOAC.

CRediT authorship contribution statement

Daniel Ali: Conceptualization, Methodology, Writing - original draft. **Caren Regine Zeiger:** Resources, Writing - original draft. **Muhammad Mohsin Azim:** Writing - review & editing. **Hilde Lea Lein:** Writing - review & editing. **Karina Mathisen:** Conceptualization, Writing - review & editing, Supervision, Funding acquisition.

Declaration of competing interest

The authors declare that they have no known competing financial interests or personal relationships that could have appeared to influence the work reported in this paper.

Acknowledgements

The authors would like to acknowledge the Norwegian University of Science and Technology for financial support. Syverin Lierhagen is thanked for conducting ICP-MS experiments.

Appendix A. Supplementary data

Supplementary data to this article can be found online at <https://doi.org/10.1016/j.micromeso.2020.110364>.

References

- [1] A.F. Ojo, J. Dwyer, J. Dewing, P.J. O'Malley, A. Nabhan, *J. Chem. Soc., Faraday Trans.* 88 (1992) 105–112.
- [2] Z. Chen, S. Zhu, P. Li, X. Li, Y. Xu, Y. Dong, W. Song, X. Yi, W. Fang, *CrystEngComm* 19 (2017) 5275–5284.
- [3] N. Danilina, F. Krumeich, J.A. van Bokhoven, *J. Catal.* 272 (2010) 37–43.
- [4] M. Westgård Erichsen, S. Svelle, U. Olsbye, *J. Catal.* 298 (2013) 94–101.
- [5] G.F. Froment, *Catal. Rev.* 50 (2008) 1–18.
- [6] M. Milina, S. Mitchell, P. Crivelli, D. Cooke, J. Pérez-Ramírez, *Nat. Commun.* 5 (2014) 3922.
- [7] H. Yang, Z. Liu, H. Gao, Z. Xie, *J. Mater. Chem.* 20 (2010) 3227–3231.
- [8] A. Feliczak-Guzik, *Microporous Mesoporous Mater.* 259 (2018) 33–45.
- [9] H. Song, Z. Liu, W. Xing, Z. Ma, Z. Yan, L. Zhao, Z. Zhang, X. Gao, *Appl. Petrochem. Res.* 4 (2014) 401–407.
- [10] S.U.H. Bakhtiar, X. Wang, S. Ali, F. Yuan, Z. Li, Y. Zhu, *Dalton Trans.* 47 (2018) 9861–9870.
- [11] J. Qi, Q. Jin, K. Zhao, T. Zhao, *J. Porous Mater.* 22 (2015) 1021–1032.
- [12] C.H. Christensen, K. Johannsen, E. Törnqvist, I. Schmidt, H. Topsøe, C. H. Christensen, *Catal. Today* 128 (2007) 117–122.
- [13] S.H. Newland, W. Sinkler, T. Mezza, S.R. Bare, M. Carravetta, I.M. Haies, A. Levy, S. Keenan, R. Raja, *ACS Catal.* 5 (2015) 6587–6593.
- [14] Q. Sun, N. Wang, G. Guo, X. Chen, J. Yu, *J. Mater. Chem. A* 3 (2015) 19783–19789.
- [15] G. Guo, Q. Sun, N. Wang, R. Bai, J. Yu, *Chem. Commun.* 54 (2018) 3697–3700.
- [16] Y. Fan, H. Xiao, G. Shi, H. Liu, X. Bao, *J. Catal.* 285 (2012) 251–259.
- [17] K. Mathisen, M. Stockenhuber, D.G. Nicholson, *Phys. Chem. Chem. Phys.* 11 (2009) 5476–5488.
- [18] K. Utcharyajit, S. Wongkasemjit, *Microporous Mesoporous Mater.* 135 (2010) 116–123.
- [19] Y. Wan, C.D. Williams, C.V.A. Duke, J.J. Cox, *J. Mater. Chem.* 10 (2000) 2857–2862.
- [20] C.A. Schneider, W.S. Rasband, K.W. Eliceiri, *Nat. Methods* 9 (2012) 671.
- [21] R.W. Grosse-Kunstleve, S.S. Prokic, M.M.J. Treacy, J.B. Higgins, C. Baerlocher, *Database of Zeolite Structures*, 2020.
- [22] J. Yoon, S. Hwa, Y.H. Kim, S.-E. Park, J.-S. Chang, *Bull. Kor. Chem. Soc.* 26 (2005) 558–562.
- [23] S.H. Jung, J.-S. Chang, J.S. Hwang, S.-E. Park, *Microporous Mesoporous Mater.* 64 (2003) 33–39.
- [24] N. Danilina, S.A. Castelanelli, E. Troussard, J.A. van Bokhoven, *Catal. Today* 168 (2011) 80–85.
- [25] Y. Cui, Q. Zhang, J. He, Y. Wang, F. Wei, *Particuology* 11 (2013) 468–474.
- [26] C. Wang, M. Yang, P. Tian, S. Xu, Y. Yang, D. Wang, Y. Yuan, Z. Liu, *J. Mater. Chem. A* 3 (2015) 5608–5616.
- [27] M.E. Potter, L.N. Riley, A.E. Oakley, P.M. Mhembere, J. Callison, R. Raja, *Beilstein J. Nanotechnol.* 10 (2019) 1952–1957.
- [28] K. Terasaka, H. Imai, X. Li, *J. Adv. Chem. Eng.* 5 (2015) 138.
- [29] S.G. Hedge, P. Ratnasamy, L.M. Kustov, V.B. Kazansky, *Zeolites* 8 (1988) 137–141.
- [30] L. Kong, Z. Jiang, J. Zhao, J. Liu, B. Shen, *Catal. Lett.* 144 (2014) 1609–1616.
- [31] K. Utcharyajit, S. Wongkasemjit, *Microporous Mesoporous Mater.* 135 (2010) 116–123.
- [32] M. Thommes, K. Kaneko, V. Neimark Alexander, P. Olivier James, F. Rodriguez-Reinoso, J. Rouquerol, S.W. Sing Kenneth, *Pure Appl. Chem.* 87 (2015) 1051.

- [33] A.K. Singh, R. Yadav, V. Sudarsan, K. Kishore, S. Upadhyayula, A. Sakthivel, *RSC Adv.* 4 (2014) 8727–8734.
- [34] L. Gómez-Hortigüela, C. Márquez-Álvarez, M. Grande-Casas, R. García, J. Pérez-Pariante, *Microporous Mesoporous Mater.* 121 (2009) 129–137.
- [35] L. Kubelková, S. Beran, J.A. Lercher, *Zeolites* 9 (1989) 539–543.
- [36] B.P.C. Hereijgers, F. Bleken, M.H. Nilsen, S. Svelle, K.-P. Lillerud, M. Bjørgen, B. M. Weckhuysen, U. Olsbye, *J. Catal.* 264 (2009) 77–87.
- [37] W. Dai, G. Wu, L. Li, N. Guan, M. Hunger, *ACS Catal.* 3 (2013) 588–596.
- [38] U. Olsbye, S. Svelle, M. Bjørgen, P. Beato, T.V.W. Janssens, F. Joensen, S. Bordiga, K.P. Lillerud, *Angew. Chem. Int. Ed.* 51 (2012) 5810–5831.
- [39] S. Teketel, M. Westgård Erichsen, F. Lønstad Bleken, S. Svelle, K. Petter Lillerud, U. Olsbye, in: J. Spivey, K.M. Dooley, Y.-F. Han (Eds.), *Catalysis: Volume 26*, The Royal Society of Chemistry, 2014, pp. 179–217.
- [40] W. Dai, W. Kong, G. Wu, N. Li, L. Li, N. Guan, *Catal. Commun.* 12 (2011) 535–538.
- [41] J. Feng, L. Guo, Z. Wang, B. Wang, J. Wang, T. Lu, J. Xu, Y. Zhan, A. Rawal, C. Zhao, L. Han, *Chemistry* 4 (2019) 10520–10524.
- [42] H. Hajfarajollah, S. Askari, R. Halladj, *React. Kinet. Mech. Catal.* 111 (2014) 723–736.
- [43] S. Seelan, A.K. Sinha, *J. Mol. Catal. Chem.* 215 (2004) 149–152.
- [44] C.M. López, K. Rodríguez, B. Méndez, A. Montes, F.J. Machado, *Appl. Catal., A* 197 (2000) 131–139.
- [45] T. Masukawa, T. Komatsu, T. Yashima, *Zeolites* 18 (1997) 10–17.
- [46] R. Roldán, M. Sánchez-Sánchez, G. Sankar, F.J. Romero-Salguero, C. Jiménez-Sanchidrián, *Microporous Mesoporous Mater.* 99 (2007) 288–298.
- [47] L. Wang, C. Guo, S. Yan, X. Huang, Q. Li, *Microporous Mesoporous Mater.* 64 (2003) 63–68.
- [48] L. Guo, X. Bao, Y. Fan, G. Shi, H. Liu, D. Bai, *J. Catal.* 294 (2012) 161–170.
- [49] M. Westgård Erichsen, S. Svelle, U. Olsbye, *Catal. Today* 215 (2013) 216–223.
- [50] J. Pérez-Ramírez, C.H. Christensen, K. Egeblad, C.H. Christensen, J.C. Groen, *Chem. Soc. Rev.* 37 (2008) 2530–2542.
- [51] J.M. Campelo, F. Lafont, J.M. Marinas, M. Ojeda, *Appl. Catal., A* 192 (2000) 85–96.
- [52] F. Mohammadparast, R. Halladj, S. Askari, *Chem. Eng. Commun.* 202 (2015) 542–556.
- [53] V. Ramamurthy, K.S. Schanze, *Solid State and Surface Photochemistry*, Taylor & Francis, 2000.
- [54] G.J. Meyer, K.D. Karlin, *Molecular Level Artificial Photosynthetic Materials*, Wiley, 2009.
- [55] L.T. Yuen, S.I. Zones, T.V. Harris, E.J. Gallegos, A. Auroux, *Microporous Mesoporous Mater.* 2 (1994) 105–117.
- [56] L. Han, Y. Liu, F. Subhan, X. Liu, Z. Yan, *Microporous Mesoporous Mater.* 194 (2014) 90–96.